ELSEVIER
Thermochimica Acta 383 (2002) 21–30
thermochimica acta
www.elsevier.com/locate/tca

Calibration and desmearing of a differential thermal analysis measurement signal upon heating and cooling

A.T.W. Kempen, F. Sommer*, E.J. Mittemeijer

Max Planck Institute for Metals Research, Seestrasse 92, D-70174 Stuttgart, Germany

Received 1 June 2001; received in revised form 12 July 2001; accepted 27 July 2001

Abstract

A new calibration and desmearing method for a differential thermal analyser (DTA) upon heating and cooling is proposed. The method is based on a heat flux model of the DTA. The parameters in this model represent the DTA *independent of heating and cooling rate*, and can be determined by measuring two calibration materials. One of these should exhibit a specific heat that varies strongly, possibly non-monotonically, with temperature. Here the ferro- to paramagnetic transition (Curie point) of iron has been used. Upon application of the proposed method, the values obtained for the heat capacity of iron around the Curie temperature were found to be independent of heating or cooling rate, and in agreement with literature data. © 2002 Elsevier Science B.V. All rights reserved.

Keywords: DTA; Calibration; Desmearing; Cooling; Curie temperature

1. Introduction

Calorimetric techniques, such as differential scanning calorimetry (DSC) and differential thermal analysis (DTA) are often applied for the determination of reaction kinetics. Reaction kinetics is usually studied isothermally or isochronally (i.e. at constant heating rate) upon heating (e.g. crystallisation of amorphous alloys). Phase transitions occurring upon cooling can be of great interest as well, e.g. the austenite to ferrite transformation in steels, which is of enormous technological importance.

The well-known techniques for temperature calibration on heating [1–3] are not suitable for the temperature calibration on cooling due to the lack of appropriate calibration phase transformations in a wide temperature range. Further, smearing of the measurement signal over time occurs if the detection is slow in comparison to the occurring heat effect (thermal lag). In this paper, a simple DTA calibration *and* desmearing method is proposed for heating *and cooling* experiments. To this end, measurements on calibration materials are performed. One of these materials should exhibit a specific heat that varies strongly, possibly non-monotonically, with temperature. Here, the ferro- to paramagnetic transition (Curie point) of iron has been used.

In the following, the term DSC is exclusively reserved for power compensated DSC, i.e. when a difference in heating power is measured. The term DTA is adopted when heat flux DSC, or DTA is meant, i.e. when a temperature difference is measured.

* Corresponding author. Tel.: +49-711-2095-417; fax: +49-711-2095-420.
E-mail address: sommer@mf.mpi-stuttgart.mpg.de (F. Sommer).

PII: S0040-6031(01)00699-2

2. Calibration and desmearing methods for DTA

2.1. Heat capacity calibration

A very common method of heat capacity calibration in non-isothermal DTA is to calculate the value of the apparent heat capacity of a sample ($C_{p,s}^{app}$) assuming that the measured temperature difference is proportional to the heat capacity of the specimen [4]:

$$C_{p,s}^{app} = C_{p,cal}\frac{\Delta T_{t,s}}{\Delta T_{t,cal}}, \quad (1)$$

where $C_{p,cal}$ is the heat capacity of the calibration material (which equals the product of the number of moles of the calibration material and the literature value for the molar heat capacity of the calibration material), $\Delta T_{t,cal}$ and $\Delta T_{t,s}$ are the measurement signals from the DTA measurements on the calibration material and on the sample, respectively. Thus, determined value for the heat capacity is an *apparent* heat capacity because the influence of smearing over time (i.e. temperature) is neglected.

2.2. Temperature calibration

Standard techniques are available for temperature calibration of a scanning calorimeter in heating experiments [1–3]. The most widely used method is based on the melting of pure substances: by comparison of the measured and the literature values of the melting temperatures, a temperature correction is determined. Actually, this temperature calibration depends not only on temperature but also on heating rate, thus, for each heating rate to be used, a separate temperature calibration has to be performed [5–7] or inter- or extrapolation of calibration parameters with respect to heating rate has to be performed [1–3].

For cooling experiments at low temperatures, specific transformations are used for temperature calibration: phase transitions in liquid crystals [8,9], solidification of specific metals that show reproducible undercooling [9], and some specific solid state phase transformation in salts or organic compounds [10].

2.3. Desmearing

A vast number of publications deal with the desmearing of DSC and DTA signals. Usually, a first-order filter is used [11–13], where the values of the filter parameters do not have a physical meaning. In those cases where the geometry and the operating mode of the apparatus have been incorporated, extremely complex desmearing procedures have been proposed (e.g. [14]), that furthermore can only be applied in cases of isochronal heating only. A third kind of desmearing methods is based on electrical heating pulses: through comparison of the electrical heating pulse and the detected effect, the smearing function can be established [15–17]. This last approach requires availability of an electrical heating device for the determination of the parameters of the model description of the smearing.

2.4. Combined calibration and desmearing

In the present work, a procedure for the simultaneous (heat capacity and temperature) calibration and desmearing of a measured DTA signal upon heating and cooling is presented, based on a heat flux model of the DTA. The procedure proposed can be used for the whole temperature range. It is proposed to employ at least two calibration materials that show different behaviours for the heat capacity as function of temperature. One of these should exhibit a very strong (preferably non-monotonically) dependence of the heat capacity on temperature. Here, pure iron is applied, that shows the ferro- to paramagnetic phase transition.

The Curie temperature corresponding to the ferro- to paramagnetic phase transition shows no temperature hysteresis [18,19], in contrast to structural transformations, because it involves a transformation during which no material transport takes place. The process that governs the transformation, i.e. the change in the relative orientation of electron spins is, at a temperature far above absolute zero, extremely fast, and thus the Curie temperature is not heating- or cooling rate dependent. Experimental work on the determination of the Curie temperature of Gd with different heating- and cooling rates (spanning a range of five decades in heating- and cooling rate) indeed did not reveal any heating- and cooling rate dependence of the Curie temperature [20].

Due to the sharp increase of the heat capacity to infinity (cf. Section 4.2) at the Curie temperature, the associated DTA measurement signal is strongly smeared. Thereby, iron is very suitable as a reference material for the application of a *combined* calibration and desmearing procedure for DTA.

3. DTA heat flux model

A DTA apparatus measures the temperature difference between a sample (to be investigated) and a reference. Sample and reference are positioned symmetrically with respect to each other in a furnace. The configuration of the sample and its surroundings in the DTA apparatus is depicted in Fig. 1.

The construction of the measurement cell is such that the heat capacity of the components 2, 3, 5 and 6 together is small in comparison to the heat capacity of the specimen, in order to enhance the sensitivity and accuracy of the measurement. The reference cell comprises an empty sample pan, but is for the rest identical to the sample measurement cell.

Heat is transported from the furnace wall (1) to each of the other, depicted components, and, depending on the heat capacities of the individual components and the thermal resistances between them, heat transport occurs between (neighbouring) components. Most of the corresponding heat resistances are small, because most of the materials, from which the DTA measurement cells are built up, are metallic, and thus they have a small inner heat resistance. The sample and reference pan are often provided with ceramic liners, to prevent reaction between sample and the metallic sample pan, and thus they have a relatively large heat resistance.

Small thermal resistances can be neglected with respect to large thermal resistances in a serial circuit.

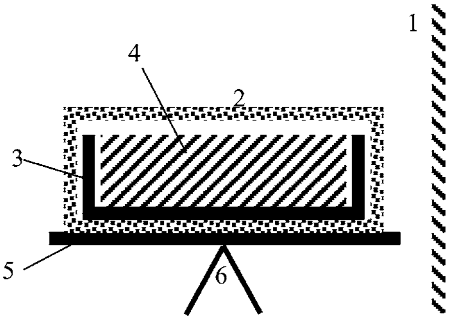

Fig. 1. Schematic presentation of the DTA apparatus: the sample measurement cell (2–6) and furnace wall (1), where (2) outer sample pan with lid, (3) inner sample pan, (4) the specimen, (5) the pan holder, and (6) is the thermocouple.

Therefore, the measurement cell as depicted in Fig. 1 can be modelled by using a very limited number of heat resistances and heat capacities; see Fig. 2.

The DTA has a symmetric configuration, with, as only difference, the sample cell, which has the heat capacity $C_{p,\mathrm{r}} + C_{p,\mathrm{s}}$, versus the reference cell, which has the heat capacity $C_{p,\mathrm{r}}$ The heat transport to the elements $\mathrm{t_r}$, r, $\mathrm{t_s}$ and s is given by:

$$\frac{\mathrm{d}q_{\mathrm{t,r}}}{\mathrm{d}t} = \frac{T_\mathrm{f} - T_{\mathrm{t,r}}}{R_\mathrm{t}} - \frac{T_{\mathrm{t,r}} - T_\mathrm{r}}{R_\mathrm{s}} = C_{p,\mathrm{t}} \frac{\mathrm{d}T_{\mathrm{t,r}}}{\mathrm{d}t}, \tag{2a}$$

$$\frac{\mathrm{d}q_\mathrm{r}}{\mathrm{d}t} = \frac{T_{\mathrm{t,r}} - T_\mathrm{r}}{R_\mathrm{s}} = C_{p,\mathrm{r}} \frac{\mathrm{d}T_\mathrm{r}}{\mathrm{d}t}, \tag{2b}$$

$$\frac{\mathrm{d}q_{\mathrm{t,s}}}{\mathrm{d}t} = \frac{T_\mathrm{f} - T_{\mathrm{t,s}}}{R_\mathrm{t}} - \frac{T_{\mathrm{t,s}} - T_\mathrm{s}}{R_\mathrm{s}} = C_{p,\mathrm{t}} \frac{\mathrm{d}T_{\mathrm{t,s}}}{\mathrm{d}t}, \tag{2c}$$

$$\frac{\mathrm{d}q_\mathrm{s}}{\mathrm{d}t} = \frac{T_{\mathrm{t,s}} - T_\mathrm{s}}{R_\mathrm{s}} = C_{p,\mathrm{s}} + C_{p,\mathrm{r}} \frac{\mathrm{d}T_\mathrm{s}}{\mathrm{d}t}, \tag{2d}$$

where T_f is the temperature of the furnace wall, T_s and T_r denote the temperatures of the sample and reference cells, and $T_{\mathrm{t,s}}$ and $T_{\mathrm{t,r}}$ are the temperatures of the thermocouples for sample cell and reference cell, respectively, $C_{p,\mathrm{s}}$ the heat capacity of the sample, $C_{p,\mathrm{r}}$ the heat capacity of the direct surroundings of the sample (i.e. the heat capacity of the reference cell), $C_{p,\mathrm{t}}$ is the heat capacity of the thermocouple and its direct surroundings, and t is the time. The measurement signals are $\Delta T_{\mathrm{t,s}} = T_{\mathrm{t,s}} - T_{\mathrm{t,r}}, T_{\mathrm{t,r}}$.

The thermocouple for the absolute temperature determination (i.e. $\mathrm{t_r}$) is not calibrated, and therefore a, temperature and heating rate independent, temperature shift of the thermocouple must be recognised as well: ΔT_{tc}.

Thus, the DTA apparatus can be represented by five (heating and cooling rate independent) parameters, further called the DTA parameters: (i) the heat resistance between the furnace wall and the thermocouples, R_t, (ii) the heat capacity of the thermocouple and its direct surroundings, $C_{p,\mathrm{t}}$, (iii) the heat capacity of the direct surroundings of the specimen, $C_{p,\mathrm{r}}$, (iv) the heat resistance R_s between sample and thermocouple (identical to the heat resistance between reference and thermocouple), and (v) the thermocouple temperature shift ΔT_{tc}.

The value of R_t is determined as a function of temperature according to the procedure described in Section 4.1. The values of $C_{p,\mathrm{r}}$, $C_{p,\mathrm{t}}$ and R_s are in principle not independent of temperature, but for a not

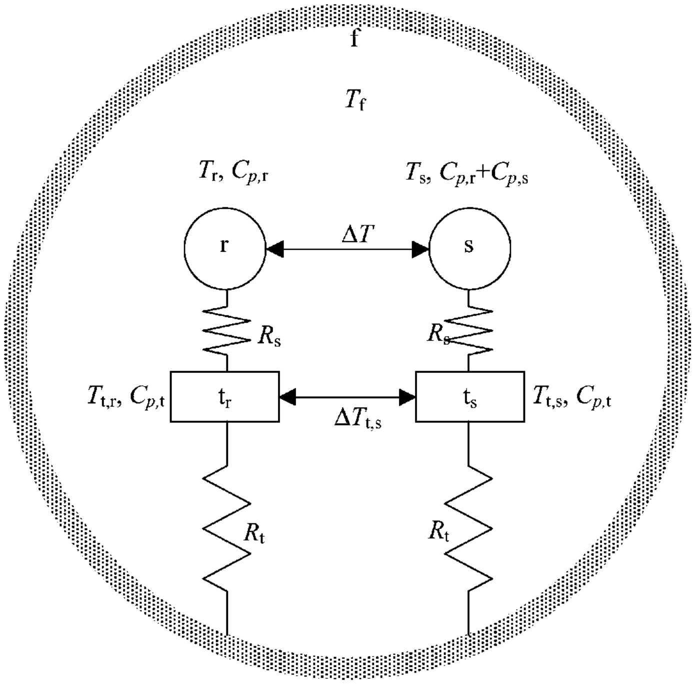

Fig. 2. Schematic presentation of a DTA apparatus. The sample and its direct surroundings (s) are coupled to the thermocouple and its surroundings (t_s) through thermal resistance R_s. This thermocouple is coupled to the furnace (f) through heat resistance R_t. The reference side (left) is identical to the sample side (right), apart from the sample. The measurement signals are: $T_{t,r}$, $\Delta T_{t,s}$ and time t.

too large temperature range, they can be taken as constants. Otherwise, the possible temperature dependence of $C_{p,r}$, $C_{p,t}$ and R_s can be accounted for by performing in this project described calibration and desmearing procedure at different temperatures (involving application of different calibration materials).

The above model of a DTA apparatus has been validated here, and the DTA parameters have been determined accordingly, by measuring the heat capacity of pure iron around the Curie temperature. The validation criterions comprise the comparison of the determined $C_{p,\mathrm{Fe}}$ values with literature values, and the comparison with each other of the $C_{p,\mathrm{Fe}}$ curves determined for the different heating and cooling rates.

4. Data evaluation

4.1. Determination of DTA parameters

The values of the five DTA parameters can be determined by DTA measurements on substances of known C_p. In this project, the values of the parameters were determined by measuring subsequently sapphire and iron, using, in both cases, four heating rates and four cooling rates. Sapphire has a molar heat capacity that smoothly changes with temperature, and iron exhibits a (heating rate independent) strongly varying molar heat capacity around the Curie temperature.

The DTA parameters $C_{p,t}$, $C_{p,r}$, and R_s can be determined by fitting as described below; the DTA parameters R_t and ΔT_{tc} follow by straightforward calculus, the parameter R_t is calculated in each iteration step and the value of ΔT_{tc} is determined after completion of the fitting process. The successive steps of the fitting procedure are as follows:

1. Initial values of the fitting parameters $C_{p,t}$, $C_{p,r}$, and R_s are prescribed. Then, using the values of $T_{t,r}$, given as function of time by the temperature program, the sapphire measurement signal ($\Delta T_{t,sap} = T_{t,sap} - T_{t,r}$) and the value for the heat capacity of sapphire ($C_{p,sap}$, c.f. Section 5), T_r, T_f, R_t and T_{sap} are calculated for each measurement

curve (each measurement curve corresponds to one heating or cooling rate) as a function of temperature, $T_{t,r}$, from the four Eqs. (2a)–(2d). The value of R_t must be independent of heating and cooling rate, and thus the average of R_t over all measurement curves is used in the further evaluation.
2. Thus, determined values of R_t, and T_f are used for the calculation of $C_{p,Fe}$ and the temperature $T_{s,Fe}$ from the DTA iron measurement curve (i.e. $T_{t,r}$ and $\Delta T_{t,Fe}$ as function of time t), using the two Eqs. (2c) and (2d). The determined results for $C_{p,Fe}$ as function of $T_{s,Fe}$ should be equal *for all heating and cooling rates*. Hence, the fit criterion is that the difference in $C_{p,Fe}$ as function of $T_{s,Fe}$, as determined at different heating and cooling rates, is small. The difference considered is defined as the product of (1) the average standard deviation for $C_{p,Fe}(T_{s,Fe})$ obtained by, firstly, determining the standard deviation in $C_{p,Fe}$ at each $T_{s,Fe}$ from the curves at different heating and cooling rates, and, secondly, averaging this standard deviation over the whole temperature range, and (2) the standard deviation of the values of the Curie temperatures (defined as the temperature at which the maximum in $C_{p,Fe}(T_{s,Fe})$ occurs) as determined at different heating and cooling rates.
3. The fit parameters $C_{p,t}$, $C_{p,r}$, and R_s are changed according to a simplex procedure [21], and the calculation sequence (1–2–3) is repeated until the fit criterion described under (2) is satisfied.
4. ΔT_{tc} is obtained as the difference between the value determined for the Curie temperature (of iron) and the literature value for the Curie temperature (of iron).

Thus, by performing DTA measurements on two calibration materials, employing different heating and cooling rates, the DTA parameters R_t, $C_{p,r}$, $C_{p,t}$, R_s and ΔT_{tc} can be determined. The two calibration materials should be selected carefully. Here, sapphire is chosen as it shows a heat capacity changing smoothly with temperature, which enables determination of R_s (see above, step (1)). Further, iron is chosen for its sharply peaked behaviour of the heat capacity. Thereby the iron measurement is in particular sensitive to smearing.

Note that the first derivatives of the measurement signals ($T_{t,r}$ and $T_{t,s} = \Delta T_{t,s} + T_{t,r}$) are used in the described procedure (Eqs. (2a) and (2c)). This enhances the sensitivity for scatter in the measurements, which is suppressed by using a moving weighted-average filter [21] for the differentials of the measurement signals.

4.2. The C_p of iron

Many references present measured values for the molar heat capacity of iron around the Curie temperature [22–30]. Most of these values were obtained by adiabatic calorimetry or by pulse heating techniques, which can be considered as the most accurate methods for measurement of C_p [31]. Here, an analytical description of $C_{p,Fe}$ is given that satisfies the data given in [22–30]. In [32], an analytical function for $C_{p,Fe}$ has been given previously. However, this formula does not describe the behaviour of $C_{p,Fe}$ of iron around the Curie temperature adequately (cf. Fig. 5).

For the analytical description of $C_{p,Fe}$, the non-magnetic contribution to $C_{p,Fe}$ as given in [32] was used: the first four terms in Eq. (3). The contribution of the magnetic ordering to $C_{p,Fe}$ is taken as given by [33,34], but here, a supplementary exponential factor is introduced, in order to better describe the experimental data given in [22–30]. Thus, the analytical description of $C_{p,Fe}$ reads:

$$C_{p,Fe} = a + bT + cT^2 + dT^{-2} + f_i \exp(e_i T^*)(T^*)^{g_i}, \tag{3}$$

where $T^* = |(T - T_c)|/T_c$, with T_c as the Curie temperature, $a = 23.5143\ \mathrm{J\,mol^{-1}\,K^{-1}}$, $b = 8.79504 \times 10^{-3}\ \mathrm{J\,mol^{-1}\,K^{-2}}$, $c = 3.535614 \times 10^{-7}\ \mathrm{J\,mol^{-1}\,K^{-3}}$, $d = 154717\ \mathrm{J\,mol^{-1}\,K}$, and e to g are parameters to be determined in this study. The label i equals 1 if $T < T_c$, and equals 2 if $T \geq T_c$. This equation was fitted to the literature $C_{p,Fe}$ data, as given in [22–30], leading to values for the fitting parameters e_i, f_i and g_i (Table 1).

Table 1
Values of the fit parameters, e_i, f_i ($\mathrm{J\,mol^{-1}\,K^{-1}}$) and g_i, obtained from fitting Eq. (3) to literature data [22–30] where every single data set was shifted such that $T_c = 1043$ K [32][a]

e_1	−5.0323	e_2	−7.0110
f_1	15.9226	f_2	12.0728
g_1	−0.1577	g_2	−0.1123

[a] The parameters e_1, f_1 and g_1 hold for $T < T_c$, and e_2, f_2 and g_2 hold for $T = T_c$.

4.3. The C_p of sapphire

The molar heat capacity of sapphire has been adopted as given in [35]:

$$C_{p,\mathrm{sap}} = \alpha_0 + \alpha_1(T - T_0) + \alpha_2(T - T_0)^2 + \alpha_3(T - T_0)^3 + \alpha_4(T - T_0)^4 + \alpha_5(T - T_0)^5, \quad (4)$$

where $T_0 = 273.15$ K, and the parameters $\alpha_0 = 73.10$ J mol^{-1} K^{-1}, $\alpha_1 = 0.2477$ J mol^{-1} K^{-2}, $\alpha_2 = -6.321 \times 10^{-4}$ J mol^{-1} K^{-3}, $\alpha_3 = 9.760 \times 10^{-7}$ J mol^{-1} K^{-4}, $\alpha_4 = -7.967 \times 10^{-10}$ J mol^{-1} K^{-5} and $\alpha_5 = 2.624 \times 10^{-13}$ J mol^{-1} K^{-6}.

5. Experimental

Using a Netzsch DSC 404C (which, according to the definition in Section 1, is a DTA apparatus), equipped with the DSC C_p sensor, a high temperature furnace (up to 1773 K), and Pt–10%Rh/Pt thermocouples, three subsequent runs were performed: with an empty sample pan, with a sapphire sample (of purity 99.99%) and with an iron sample (of purity 99.98%). The sapphire and the iron samples were disc shaped with a diameter of about 5 mm, and a thickness of about 1.5 mm. These three measurements were performed using the same reference and sample pans, and the same temperature–time program, employing a number of heating and cooling rates.

In order to correct for small differences between the sample cell and the reference cell, the measurement signal $\Delta T_{\mathrm{t,s}}$ for the empty run (which equals zero in the ideal case) is subtracted from the corresponding measurement curves recorded from sapphire and iron. The resulting values are considered to represent the true measurement signal, $\Delta T_{\mathrm{t,s}}$.

The data analysis is performed as described in Section 4.1, using as input data the Curie temperature of iron, $T_c = 1043$ K [32], and the (molar) heat capacity of sapphire (cf. Section 4.3).

6. Results and discussion

From the measurements as described in Section 5, the *apparent* molar heat capacity of iron was calculated, using Eq. (1), taking the measurement with sapphire as the calibration measurement.

Crudely speaking, the presented $C_{p,\mathrm{Fe}}^{\mathrm{app}}$ (Fig. 3) is proportional to the measured signal ($\Delta T_{\mathrm{t,Fe}}$) divided by the heating or cooling rate (cf. Eq. (2a)). It is clear from Fig. 3 that the apparent molar heat capacity as

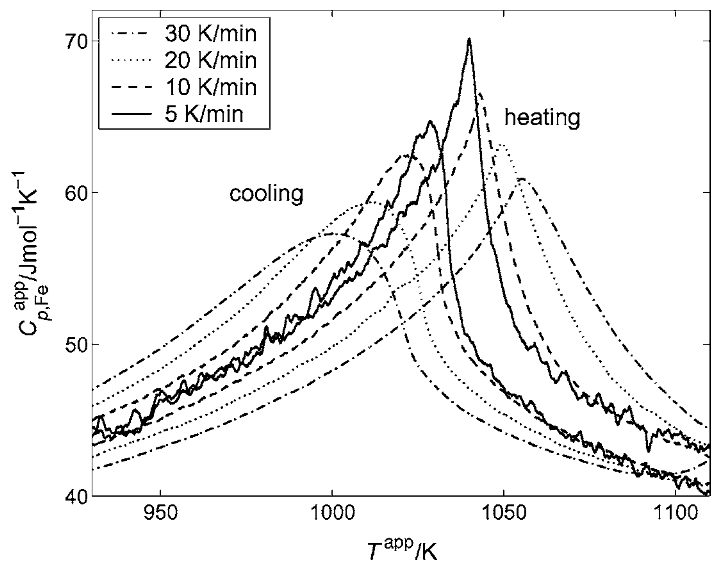

Fig. 3. Apparent molar heat capacity (cf. Eq. (1)) of pure iron as determined from the DTA measurements at various heating and cooling rates, using sapphire as calibration material.

determined using Eq. (1), strongly depends on the heating or cooling rate. The real heat capacity is independent of heating rate (cf. Section 2.2). The erroneous heating rate dependence of $C_{p,\mathrm{Fe}}^{\mathrm{app}}$ exhibited in Fig. 3 is caused by the smearing and the temperature shift inherent to the DTA apparatus. Next, the correction method for the smearing and temperature shift, as proposed in Section 4.1, was applied to the measured data.

6.1. The C_p of iron

Application of the correction method for smearing and temperature shift to the measured data, $\Delta T_{\mathrm{t,sap}}$ and $\Delta T_{\mathrm{t,Fe}}$ as function of $T_{\mathrm{t,r}}$, as described in Section 4.1, led to results for the real molar heat capacity shown in Fig. 4, and the values for the DTA parameters given in Table 2.

Indeed, the result for $C_{p,\mathrm{Fe}}$ as derived from the measurements is independent of heating and cooling rate. The ordinate values of the curves presented in Fig. 4, as averaged over the heating and cooling rate, are plotted in Fig. 5, together with literature data of the molar heat capacity of iron [22–30], and the analytical descriptions given by [32] and Eq. (3).

The shape of the $C_{p,\mathrm{Fe}}$ curve derived from the measurements agrees very well with the shape of the curve representing the literature data. The measured value for $C_{p,\mathrm{Fe}}$ is about 2 J mol^{-1} K^{-1} lower than the literature value. This difference is within the experimental accuracy of a C_p determination by DTA in the temperature range considered; in particular it

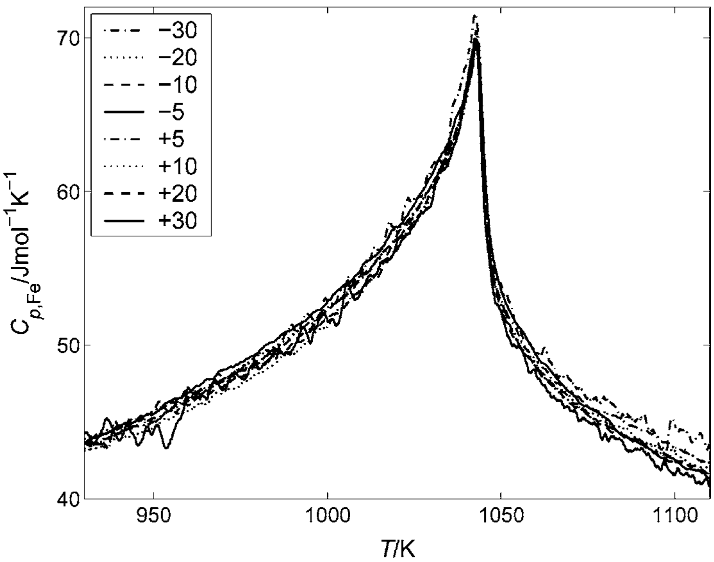

Fig. 4. True molar heat capacity of pure iron, $C_{p,\mathrm{Fe}}$, as obtained after application of the correction procedure for smearing and temperature shift, for various applied heating and cooling rates.

Table 2
DTA parameters as determined by fitting ($C_{p,\mathrm{t}}$, $C_{p,\mathrm{r}}$, and R_s), and by direct calculus calculation (ΔT_{tc} and R_t) (cf. Section 4.1)[a]

$C_{p,\mathrm{t}}$ (J K^{-1})	$C_{p,\mathrm{r}}$ (J K^{-1})	R_s (K J^{-1})	ΔT_{tc} (K)	T (K)	R_t (K J^{-1})	$C_{p,\mathrm{sap}}$ (J K^{-1})	$C_{p,\mathrm{Fe}}$ (J K^{-1})
0.0676	0.0326	61.2359	7.1	1000	64.8526	0.1028	0.2255
				1025	62.2368	0.1032	0.2527
				1050	59.6920	0.1035	0.2225
				1075	57.2239	0.1038	0.1993

[a] Further, the heat capacities of the sapphire and the iron sample are given as determined from the number of moles ($n_{\mathrm{Fe}} = 4.2 \times 10^{-3}$ mol; $n_{\mathrm{sap}} = 8.2 \times 10^{-4}$ mol) and the molar heat capacity, i.e. Eqs. (3) and (4). The values of R_t, $C_{p,\mathrm{sap}}$ and $C_{p,\mathrm{Fe}}$ are given for different temperatures.

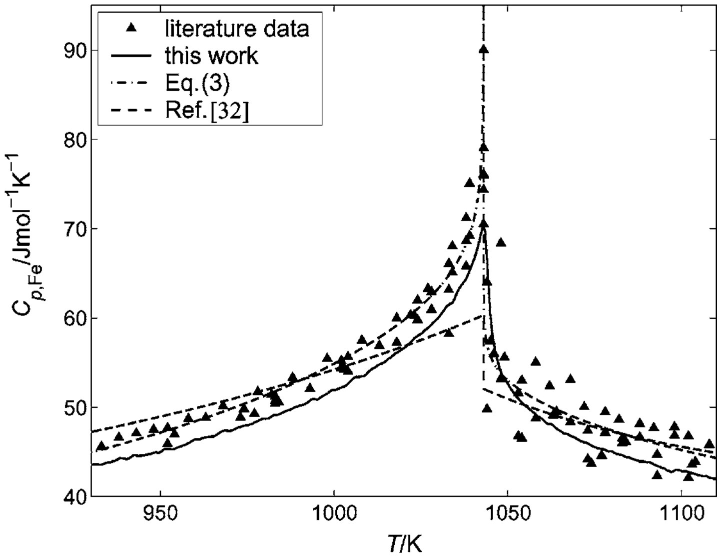

Fig. 5. Molar heat capacity of iron as determined in this work measured (—) the average over all heating and cooling rates calculated from the plots shown in Fig. 4; from literature [22–30] where every single data set was shifted such that $T_c = 1043$ K (▲); as described by Eq. (3) (· - - · -); and as given in [32] (- - -).

should be noted that low heating and cooling rates i.e. 5 and 10 K min^{-1} were included in the analysis, which normally affects the experimental accuracy. That the small discrepancy is of systematic character, might be due to the *non-metallic* nature of the calibration substance sapphire as compared to the *metallic* nature of the material (iron) investigated.

The line representing the literature data as depicted in Fig. 5 has been obtained by fitting Eq. (3) to the literature data [22–30], where every single data set was shifted such that $T_c = 1043$ K [32]. The values of the corresponding fit parameters are given in Table 1.

As follows from Fig. 5, the literature data for $C_{p,\mathrm{Fe}}$ can be described very well by Eq. (3). The value of parameter g used for this description, should be between 0 and -0.16 [33]. The present result satisfies this requirement, but it should be noted that the in this work applied exponential factor incorporated in the present description (cf. Eq. (3)) can influence the value of g.

6.2. The DTA parameters

The DTA parameters as determined from the sapphire and iron measurements by the procedure described in Section 4.1 have been given in Table 2.

The presented heat capacities, $C_{p,\mathrm{t}}$ and $C_{p,\mathrm{r}}$, are smaller than the heat capacities of the samples, $C_{p,\mathrm{sap}}$ and $C_{p,\mathrm{Fe}}$ which is plausible, cf. first paragraph of Section 3. The value obtained for the thermocouple shift ΔT_{tc} is also plausible. The temperature dependent heat resistance R_{t} becomes smaller with increasing temperature, which is understandable recognising that with increasing temperature, the contribution of radiation to the heat transport process increases.

6.3. Influence of smearing

To demonstrate the influence of the smearing, the apparent molar heat capacity of iron (as defined according to Eq. (1)) has been calculated from the true molar heat capacity of iron (adopting Eq. (3); cf. Section 6.1), applying the smearing according to Eq. (2). The calculation is performed by numerical integration (using a fourth-order Runge–Kutta method [21]) of the Eq. (2) and adopting the DTA parameters as given in Table 2. Results for the heating and cooling rates of 30 K min^{-1}are shown in Fig. 6. The experimental $C_{p,\mathrm{Fe}}^{\mathrm{app}}$ (derived from the measurements using Eq. (1), see also Fig. 3) is shown in Fig. 6 as well.

The shape of the as-calculated smeared $C_{p,\mathrm{Fe}}^{\mathrm{app}}$ peaks agrees very well with the shape of the experimentally

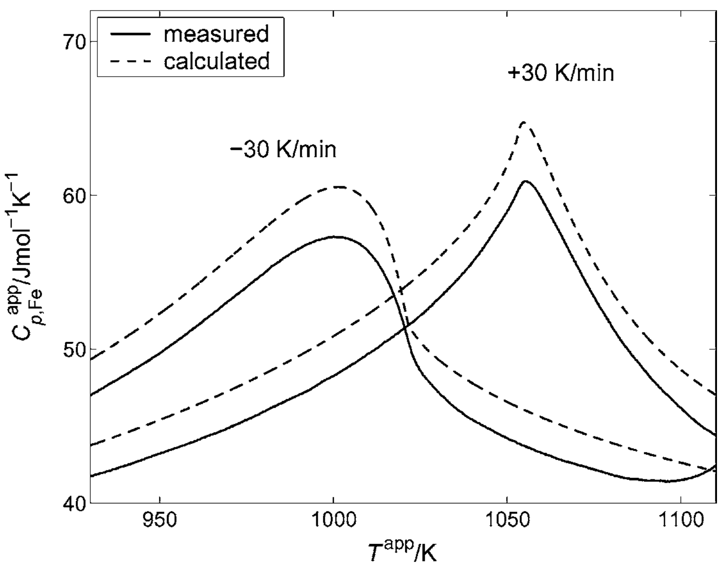

Fig. 6. The *apparent* molar heat capacity as calculated directly from the measurement using Eq. (1) (—) and as calculated from the *true* molar heat capacity $C_{p,\mathrm{Fe}}$ (Section 6.1) applying the smearing according to Eq. (2) using the DTA parameters given in Table 2 (- - -) for heating and cooling at 30 K min^{-1}.

determined $C_{p,\mathrm{Fe}}^{\mathrm{app}}$ peaks. The systematic, small difference between ordinate values has already been discussed in Section 6.1. Hence, the DTA model presented here, can be used both for the desmearing of experimentally smeared peaks (cf. Fig. 4), as well as the mathematical smearing of real C_p peaks (simulation of DTA experiment).

The observed difference between $C_{p,\mathrm{Fe}}^{\mathrm{app}}$ peak shapes for heating and cooling is not caused by the instrumental smearing because the smearing is symmetrical with respect to the heating or cooling rate applied (cf. Eq. (2)). The asymmetry in the $C_{p,\mathrm{Fe}}$ peak in combination with smearing on cooling leads to a strong asymmetry in the apparent heat capacity peak obtained on cooling, whereas smearing upon heating counteracts the asymmetry in $C_{p,\mathrm{Fe}}$, leading to a less distinct asymmetry in the apparent heat capacity peak obtained on heating, see Fig. 6.

7. Conclusions

DTA equipment can be modelled by a heat flux model, incorporating only five parameters that are *independent* of heating or cooling rate. On this basis measured DTA curves can be, simultaneously, both calibrated with respect to heat capacity and temperature and corrected for the heating and cooling rate dependent smearing of the signal. Thus, a general procedure is available, allowing for calibration and desmearing upon heating *and cooling*.

The model parameters can be determined by measuring the heat capacity of two calibration materials: one that features a heat capacity only smoothly varying with temperature, and one that features a heat capacity strongly varying with temperature. This heat capacity variation should be independent of heating and cooling rate. Here, sapphire and iron were used as calibration materials, where the ferro- to paramagnetic transformation in iron caused the, heating- and cooling rate independent, strong variation of the heat capacity. The molar heat capacity of sapphire and the Curie temperature of iron were used as input data. Fitting of the model yielded the model parameters and the true molar heat capacity of iron as a function of temperature. The course of the true molar heat capacity curve of iron around the magnetic transition agrees well with literature data, thereby validating the proposed calibration and desmearing procedure.

References

[1] E. Gmelin, S.M. Sarge, Thermochim. Acta 347 (2000) 9.
[2] G.W.H. Höhne, H.K. Cammenga, W. Eysel, E. Gmelin, W. Hemminger, Thermochim. Acta 160 (1990) 1.
[3] H.K. Cammenga, W. Eysel, E. Gmelin, W. Hemminger, G.W.H. Höhne, S.M. Sarge, Thermochim. Acta 219 (1993) 333.
[4] R.F. Speyer, Thermal Analysis of Materials, Marcel Dekker, New York, 1994.
[5] J.D. Menczel, J. Thermal Anal. 49 (1997) 193.
[6] Pyris Software, 3.7 Edition, Perkin Elmer, 1999.
[7] Thermal Analysis, Software 4.0, beta Edition, Netzsch, Selb, 1999.
[8] G.W.H. Höhne, J. Schawe, C. Schick, Thermochim. Acta 221 (1993) 129.
[9] C. Schick, G.W.H. Höhne, Thermochim. Acta 187 (1991) 351.
[10] S.M. Sarge, G.W.H. Höhne, H.K. Cammenga, W. Eysel, E. Gmelin, Thermochim. Acta 361 (2000) 1.
[11] H.J. Flammersheim, N. Eckardt, W. Kunze, Thermochim. Acta 187 (1991) 269.
[12] S. Wiesner, E. Woldt, Thermochim. Acta 187 (1991) 357.
[13] G.P. Krielaart, S. van der Zwaag, Mat. Sci. Tech. 14 (1998) 10.
[14] W. Poessnecker, Thermochim. Acta 187 (1991) 309.
[15] K.H. Schönborn, Thermochim. Acta 69 (1983) 103.
[16] X.Y. Wang, Y.K. Hou, C.N. Wu, Thermochim. Acta 123 (1988) 177.
[17] M.M. Nicolaus, Thermochim. Acta 151 (1989) 345.
[18] E. Kneller, Ferromagnetismus, 1st Edition, Springer, Berlin, 1962.
[19] R.M. Bozorth, Ferromagnetism, 2nd Edition, D. van Nostrand Co., Toronto, 1951.
[20] Y.H. Jeong, D.J. Bae, T.W. Kwon, I.K. Moon, J. Appl. Phys. 70 (1991) 6166.
[21] W.H. Press, S.A. Teukolsky, W.T. Vetterling, B.P. Flannery, Numerical Recipes in C, Cambridge University Press, NY, 1997.
[22] M. Braun, Ph.D. Thesis, Universität zu Köln, 1964.
[23] J. Korn, R. Kohlhaas, Z. Angew. Phys. 26 (1969) 119.
[24] P.R. Pallister, J. Iron Steel Inst. 161 (1949) 87.
[25] D.C. Wallace, P.H. Sidles, G.C. Danielson, J. Appl. Phys. 31 (1960) 168.
[26] D.L. McElroy, Ph.D. Thesis, Tennessee, 1957.
[27] M.L. Picklesimer, Ph.D. Thesis, Tennessee, 1954.
[28] J. Rogez, J. Lecoze, Rev. Phys. Appl. 15 (1980) 341.
[29] W. Bendick, W. Pepperhoff, Acta Met. 30 (1982) 679.
[30] J.H. Awbery, E. Griffiths, Proc. R. Soc. A 174 (1940) 1.
[31] Y.S. Touloukian, E.H. Buyco, Specific Heat, Metallic Elements and Alloys, Vol. 4, Plenum Press, New York, 1970.
[32] A.T. Dinsdale, Calphad 15 (1991) 317.
[33] C.N.R. Rao, K.J. Rao, Phase Transitions in Solids: An Approach to the Study of the Chemistry and Physics of Solids, McGraw-Hill, New York, 1978.
[34] A. Münster, Statistical Thermodynamics, Vol. II, Springer, Berlin, 1974.
[35] J.D. Cox, Pure Appl. Chem. 40 (1974) 391.